Spurious microwave resonance modes of superconducting device

Semester thesis

Marc-Philippe Röösli

Supervisor: Dr. Mintu Mondal

ETH Zürich
Qudev group
Prof. Dr. A. Wallraff

May 27, 2015

Abstract

During the transmission measurements of coplanar waveguide resonators, in addition to the resonator modes, we observe some spurious resonance modes visible in all transmission amplitudes. These spurious resonance modes supported by the superconducting ground plane of the device and the printed circuit board on which the sample is mounted, are detrimental to the operation and measurement of superconducting device. Here we analyse these resonance modes experimentally and present a way to shift them to higher frequencies such that they don't appear in the frequency range of interest. We also describe the problems encountered during the unsuccessful attempt to develop a finite element simulation of the sample including the printed circuit board and the sample holder.

Contents

1 Introduction

In 1984 C. H. Bennett and G. Brassard presented their quantum key distribution protocol[1], nowadays known as BB84, that achieves information theoretical security by using principal features of quantum mechanics which is impossible in classical information theory. Spurred by this the field of quantum information theory and quantum computing[2, 3] emerged developing theoretical foundation and trying to find new algorithms and procedures that make use of quantum mechanics. This progress demands for the development of physical systems implementing quantum computations. A promising system for the realisation of such experiments are superconducting qubits[4, 5] with which for example already a violation of the Bell inequality[6] was shown, giving strong evidence for the real quantum nature of this system. In order to be used for quantum information processing, superconducting qubit systems have to be sufficiently isolated from the electromagnetic environment to preserve coherence long enough for executing quantum information operations while having good control over it.[7] Superconducting qubit systems typically interact strongly with the environment, thus they are hard to isolate.[7] A widely used method is the circuit quantum electrodynamics(cQED) architecture[8, 9, 10] in which a high quality coplanar waveguide(CPW) resonator[11] is coherently coupled to the superconducting qubit[8]. The coupling to the resonator enhances coherence length far from the resonance frequency and allow for measurement of the qubit.[7] The cQED architecture is a promising candidate for scalable quantum computers but at the moment offers not yet high enough coherence times.

In this thesis the microwave properties of the superconducting device used for cQED experiments mounted on a printed circuit board(PCB) was studied. This was motivated by earlier measurements in this group which showed spurious resonance modes near the resonance frequencies of the CPW resonators on the chip. These resonance modes were visible in all transmission amplitudes and are supported by the superconducting ground plane of the device and the PCB. For simplicity, these resonance modes are later also referred to as PCB resonance modes. These resonance modes can couple to the qubits of the cQED chip and lead to an unwanted decay channel[7] reducing the coherence of the qubit system. Additionally they interfere with the desired coupling of the qubits to the CPW resonators used for the readout the qubits. In order to get good coherence length it is therefore crucial to remove those resonance modes from the relevant frequency range.

Additionally to the experimental analysis, presented in section 2, a main goal was to develop a finite element simulation of the PCB plus sample holder which could not be realized, see section 3.

2 Experimental Results

In this section we present results of transmission spectrum measurements of two coplanar waveguide (CPW) resonators on a cQED chip placed on a printed circuit board (PCB). The resonance frequencies are determined and changes upon modifying the PCB are examined.

2.1   Measurement Setup and Process

The coplanar waveguide resonators studied were realized on a 150 nm thick niobium(Nb) layer patterned with optical lithography on top of a sapphire chip. The chip is glued on a PCB and connected by bond wires, see Fig. 1 a). The PCB has up to 16 coaxial ports out of which only four were used during the measurements. The PCB is screwed onto a sample holder and covered with a lid, as can be seen in Fig. 1 b)-d), both consisting of copper (Cu). The sample holder is fixed at the lower end of a dipstick. There are 16 coaxial cables connecting the sample to the top of the dipstick. During the measurements the dipstick is lowered into a tank filled with liquid helium (He).

The measurements were done using a 4-port network analyser (PNA). Before measuring, the network analyser was calibrated with the help of an external electric driven calibration device enabling an automatic calibration of all 4 ports. This calibration is only valid up to the end of the coaxial cables connecting the network analyser to the top of the dipstick. To account for losses from the cables in the dipstick and the PCB a reference measurement with a short-circuited PCB was made. The measured data was corrected by subtracting the reference transmission amplitude from port 2 to port 1, i.e. S_{12}, in dB for every transmission amplitude of the measured raw data.

Fig. 1: a) PCB with sapphire chip, b) PCB on sample holder covered with lid, c) sample holder, d) lid with side visible which faces the PCB

Following settings were used for the network analyser for all measurements in this report as well as the calibration: number of points: 2000; IF-Bandwidth: 100 kHz; power: −8.00 dBm; averaging factor: 100 (20 during the calibration). The calibration was done in the frequency range from 300 kHz to 20 GHz.

Measurements were conducted on two different PCBs. On the first one the sapphire chip was glued on top with no alteration. In the second PCB a hole was cut below the chip, leaving only a small margin where the chip was glued. From now on they are referred to as no-cut and cut PCB respectively.

During the measurements ports 1 and 2 were connected to the first CPW resonator and ports 3 and 4 to the second one, and the transmission matrix S was recorded. Therefore transmission through the first (second) CPW resonator corresponds to transmission amplitude S_{12} (S_{34}).
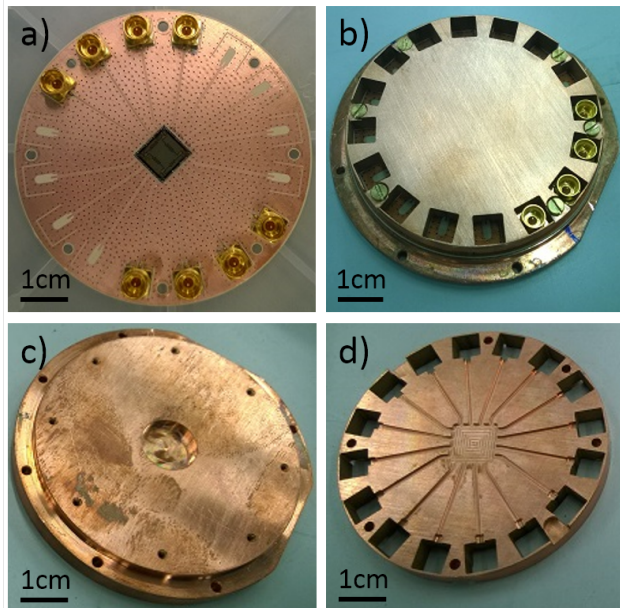
2.2   Transmission Spectrum

In Fig. 2 the transmission spectrum is plotted for the no-cut PCB. The four transmission amplitudes correspond to the transmission through both resonators, S_{12} and S_{34}, and cross-coupling transmission between ports 4 and 1, S_{14}, and ports 3 and 2, S_{23}. There is a peak observable at around 7.5 GHz and 9.5 GHz respectively, in the transmission of the respective CPW resonator. These peaks correspond to the fundamental resonance of the resonators.
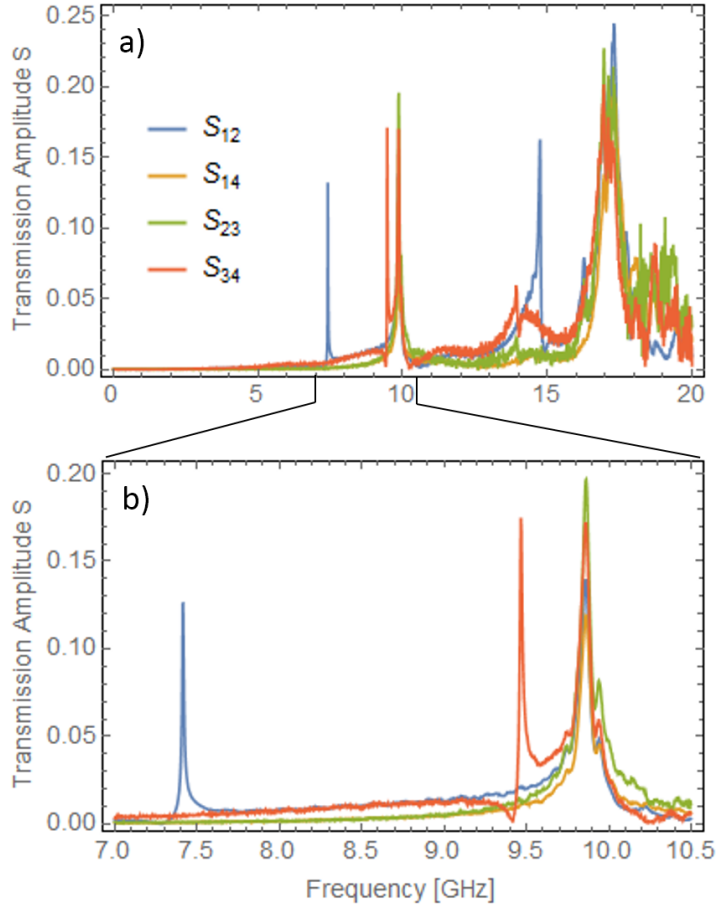

Fig. 2: Transmission spectrum through both resonators, S_{12}, S_{34}, as well as cross-coupling, S_{14}, S_{23}, recorded for the device mounted on the PCB which has no cut underneath the chip. In b) a part of the spectrum shown in a) is enlarged.

At 9.8 GHz another resonance is visible in all transmission amplitudes which is therefore understood as a resonance supported by the superconducting ground plane of the device and the PCB. This PCB resonance is very close to the fundamental resonance frequency of the second CPW resonator. When using this CPW resonator as part of a circuit quantum electrodynamics (cQED)[8] coupled to a qubit[4, 5], the PCB resonance will also couple to the qubit and lead to an additional unwanted decay channel of the qubit. This will disturb the measurements of the qubit which are done by letting the qubit decay into the CPW resonance. Secondly, the additional decay channel will reduce the coherence time of the qubit system.
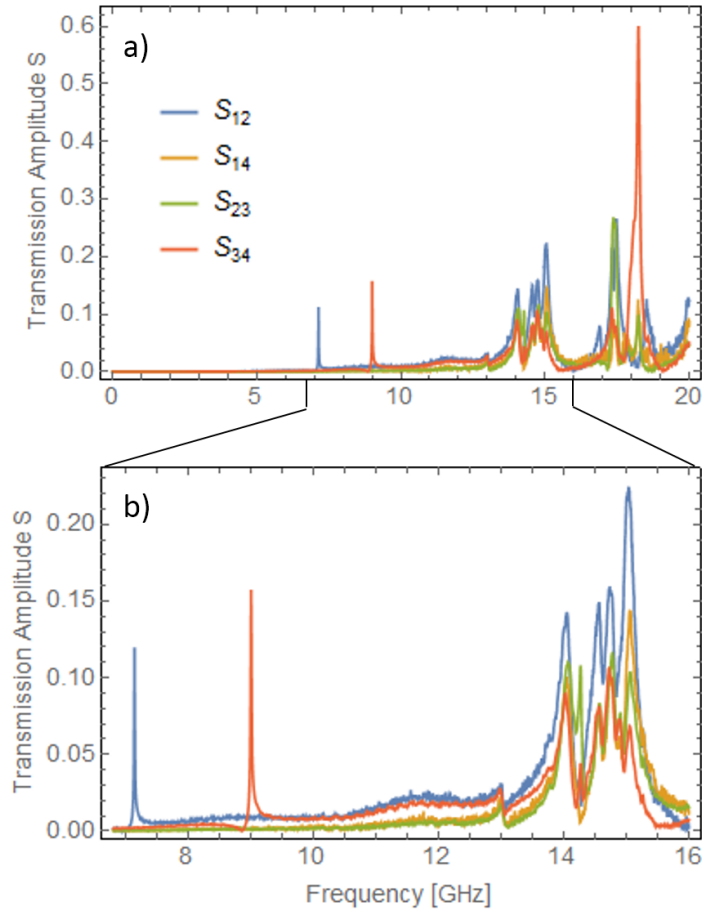
Fig. 3: Transmission spectrum through both resonators, S_{12}, S_{34}, as well as cross-coupling, S_{14}, S_{23}, recorded for the device mounted on the PCB which has a hole cut out underneath the chip. Graphic b) shows a zoom on part of the spectrum shown in a).

In the transmission spectrum depicted in Fig. 2 also higher harmonic resonance modes are visible. The resonance at around 15 GHz in the transmission amplitude of the first resonator corresponds to the second harmonic and is approximately at the double frequency of the fundamental mode as expected. The second harmonic of the second resonator is not visible. It is probably superimposed by the higher harmonics of the PCB resonance which are observed between 16 and 20 GHz.

The transmission spectrum of the cut PCB is shown in Fig. 3. The same four transmission amplitudes were plotted as for the spectrum of the no-cut PCB in Fig. 2. Again the fundamental resonances of the CPW resonators are well noticeable in the respective transmission amplitude at around 7.1 GHz and 9 GHz respectively.

In contrast to the no-cut PCB, no resonance is visible near the two fundamental resonances of the CPW resonators in all transmission amplitudes at the same time for the cut PCB. Only at around 14 GHz a first resonance of this kind emerges which is attributed to the fundamental resonance of the PCB. Therefore we observe that for the cut PCB the PCB resonance is shifted to higher frequencies, by approximately 4 GHz compared to the no-cut

PCB, leaving both fundamental modes of the CPW resonators clearly separated and well distinguishable.

A basic qualitative theoretical explanation of the shift of the PCB resonance is found by considering a simple capacitive coupling model of the niobium plane on the chip to the PCB copper plane below the chip. Assuming this capacitance to be C and neglecting magnetic properties this gives rise to a resonance frequency $f_0^{PCB} \propto \frac{1}{\sqrt{C}}$, compare to [11]. If we now cut out the PCB copper plan below the chip, the capacitance C will be reduced and as a consequence the PCB resonance frequency f_0^{PCB} will increase as is observed in the experimental result.

As for the no-cut PCB we can also observe some higher mode resonances in the case of the cut PCB. The second harmonic of the second resonator is well distinguishable at the double fundamental frequency at roughly 18 GHZ. Above 14 GHz we can see the higher modes of the PCB resonance which are seen in all four traces simultaneously. The second harmonic resonance of the first resonator is probably superimposed with the PCB resonances as it is not apparent.

2.3 Resonator Properties

The fundamental resonance frequency of a CPW resonator follows the standing wave condition with both ends fixed, $\lambda_0 = 2l$, and is given by

$$f_0 = \frac{c}{\sqrt{\epsilon_{\text{eff}}}} \frac{1}{2l} \tag{1}$$

where l is the length of the resonator, λ_0 the wavelength of the fundamental resonance, c the speed of light in vacuum, and ϵ_{eff} the effective permittivity of the resonator [11].

The modulus of the transmission amplitude squared, $|S|^2$, of a CPW resonator follows a Lorentzian line shape

$$F_{\text{Lorentz}}(f) = A \frac{\delta f}{(f - f_0)^2 + \delta f^2/4} + y_0 \tag{2}$$

where δf is the full width at half maximum (FWHM) at the resonance frequency f_0, A a proportionality factor and y_0 a offset parameter [11]. From this the quality factor of the resonance can be determined as the ratio of the resonance frequency and the FWHM [11]

$$Q = \frac{f_0}{\delta f}. \tag{3}$$

The resonances of the fundamental modes of the resonators were fitted with a Lorentzian according to Eq. (2). The resulting curve for the case of the no-cut PCB is shown in Fig. 4. The fundamental frequencies extracted form the fit are $f_0^{(1)} = 7.415$ GHz for the first and $f_0^{(2)} = 9.467$ GHz for the second resonator. For the the quality factors we get, according to Eq. (3), $Q^{(1)} = 940$ and $Q^{(2)} = 650$.

For the transmission through the second resonator, S_{34}, the fitting range was chosen nar-
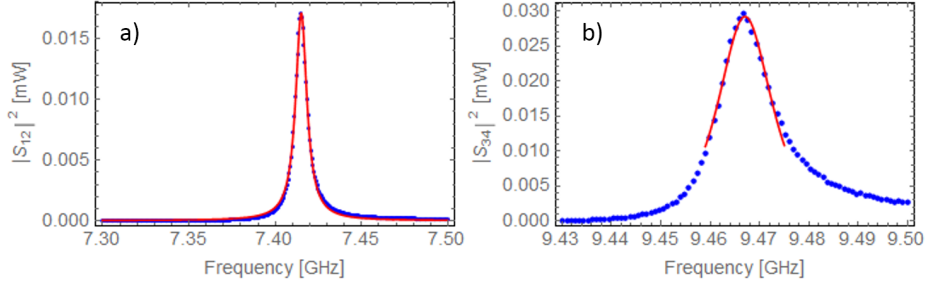
Fig. 4: For the case of the no-cut PCB: a) Transmission of the first resonator, $|S_{12}|^2$, fitted with a Lorentzian line shape around the fundamental resonance. Yields a resonance frequency $f_0^{(1)} = 7.415\,\mathrm{GHz}$ and a quality factor $Q^{(1)} = 940$. b) Transmission of the second resonator, $|S_{34}|^2$, fitted with a Lorentzian line shape around the fundamental resonance. Yields a resonance frequency $f_0^{(2)} = 9.467\,\mathrm{GHz}$ and a quality factor $Q^{(2)} = 650$.
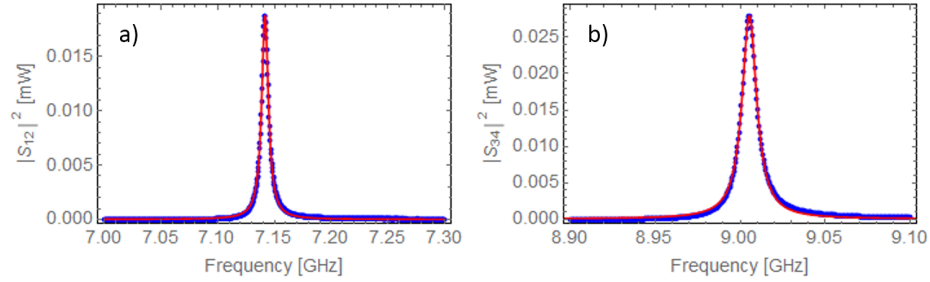

Fig. 5: For the case of the cut PCB: a) Transmission of the first resonator, $|S_{12}|^2$, fitted with a Lorentzian line shape around the fundamental resonance. Yields a resonance frequency $f_0^{(1)} = 7.142\,\mathrm{GHz}$ and a quality factor $Q^{(1)} = 1000$. b) Transmission of the second resonator, $|S_{34}|^2$, fitted with a Lorentzian line shape around the fundamental resonance. Yields a resonance frequency $f_0^{(2)} = 9.005\,\mathrm{GHz}$ and a quality factor $Q^{(2)} = 860$.

rowly around the peak. The resonance does not fully relax to zero on the right side of the resonance, resulting in some asymmetry. This is due to interference effects from the 9.9 GHz PCB mode and makes the restriction of the fitting range justifiable. However, it limits the accuracy of the determined quality factor $Q^{(2)}$.

For the cut PCB the fitted lines of the two resonances are displayed in Fig. 5. The fit yields a fundamental resonance frequency of $f_0^{(1)} = 7.142\,\mathrm{GHz}$ for the first and $f_0^{(2)} = 9.005\,\mathrm{GHz}$ for the second resonator. The quality factors are computed to be $Q^{(1)} = 1000$ and $Q^{(2)} = 860$.

For both, the no-cut and the cut PCB, there is a good agreement of the Lorentzian fit, given by Eq. (2), with the measured data on a large interval compared to the peak width, FWHM (with the already discussed exception of S_{34} for the no-cut PCB). We conclude that the measurements are in good accordance with the theory.
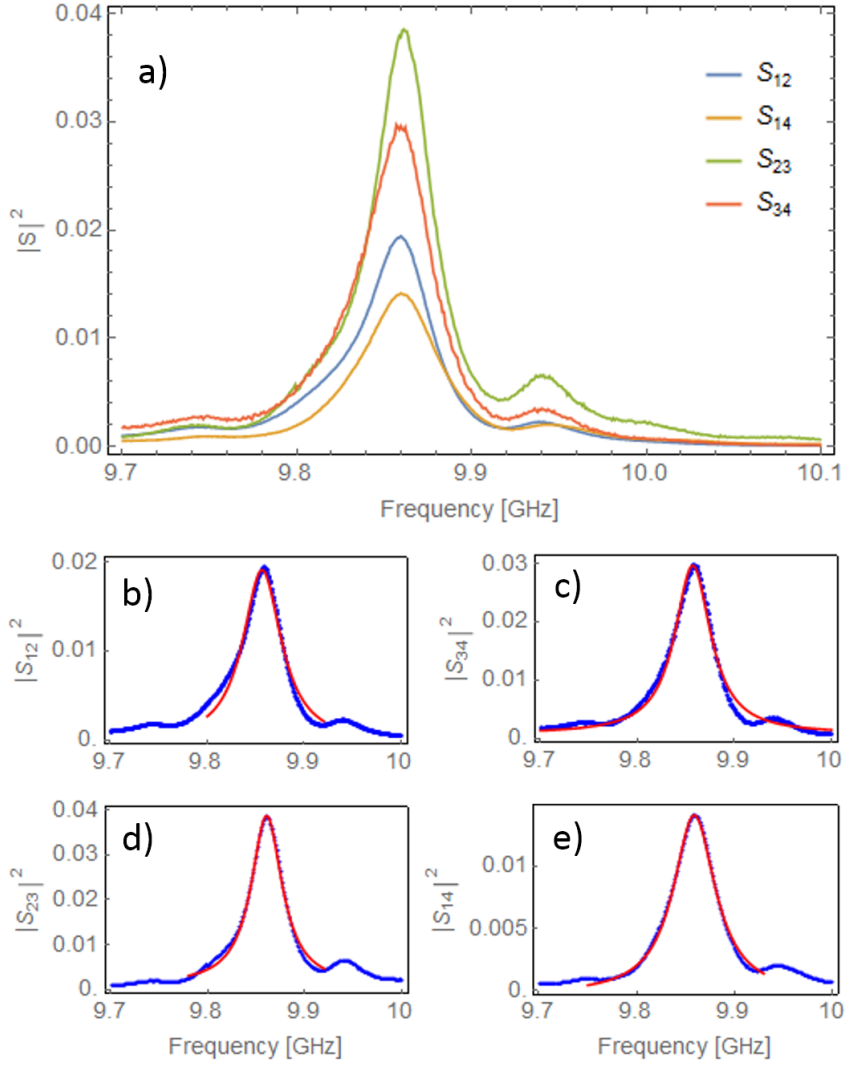
Fig. 6: For the no-cut PCB: a) Transmission spectrum $|S|^2$ of the PCB resonance of the four transmission parameters $|S_{12}|^2$, $|S_{14}|^2$, $|S_{23}|^2$ and $|S_{34}|^2$. b)-e) Lorentzian fit for each trace shown in a). Results of the fit parameters are presented in Tab. 1.

2.4   PCB-Resonance

The transmission of the PCB resonance was also fitted with a Lorentzian in order to extract the resonance frequency f_0 and the Quality factor Q according to Eq. (2) and Eq. (3). This was done for each of the four transmission parameters $|S_{12}|^2$, $|S_{14}|^2$, $|S_{23}|^2$ and $|S_{34}|^2$. The resulting curves for the no-cut PCB are shown in Fig. 6 as well as an overview of the transmission spectrum of the PCB resonance for these four traces. The same was done for the cut PCB with the result shown in Fig. 7. The resonance frequency f_0 and the quality factor Q calculated from the fits are listed in Tab. 1.

The measured data of the no-cut PCB does agree well with the Lorentzian fits. The fits of all four traces yield the same PCB resonance frequency $f_0 = 9.86\,\text{GHz}$ up to the third
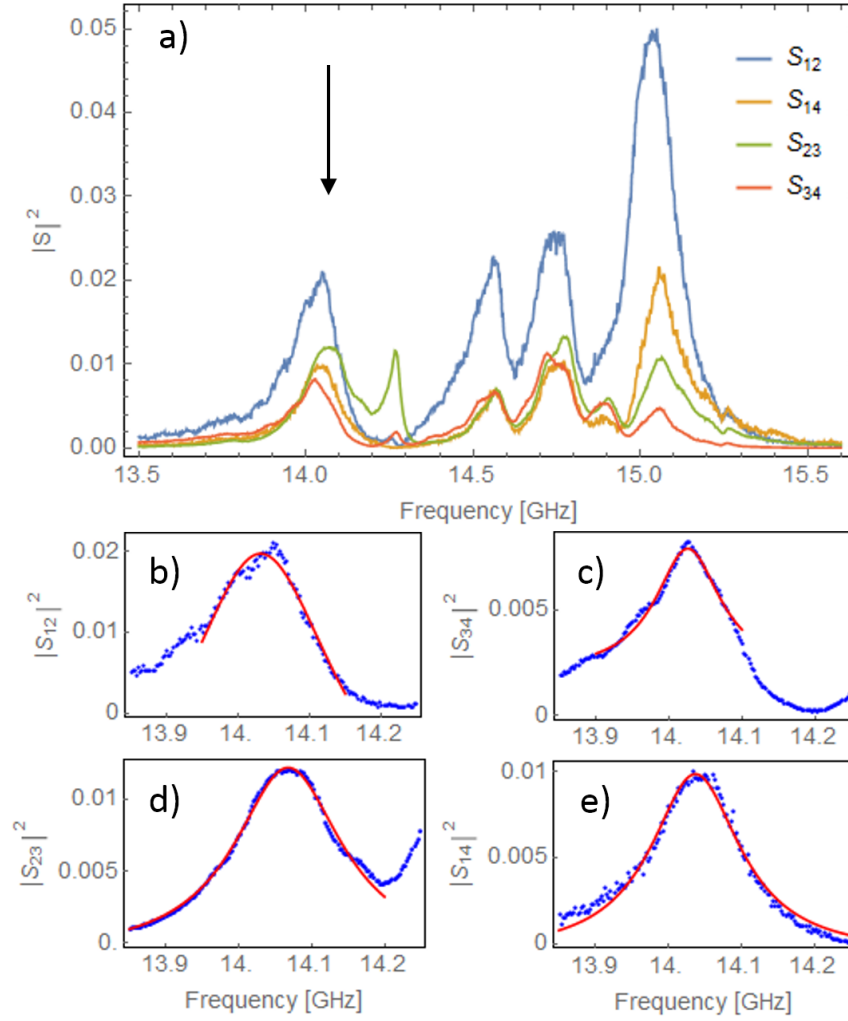
Fig. 7: For the cut PCB: a) Transmission spectrum $|S|^2$ of the PCB resonance at roughly $14\,\mathrm{GHz}$ (marked with black arrow) of the four transmission parameters $|S_{12}|^2$, $|S_{14}|^2$, $|S_{23}|^2$ and $|S_{34}|^2$. b)-e) Lorentzian fit of the PCB resonance at $14\,\mathrm{GHz}$ for each trace shown in a). Results of the fit parameters are listed in Tab. 1.

digit. The Quality factors are all around $Q = 220 \pm 30$.

For the case of the cut PCB the PCB resonance is more noisy. Still the fits agree quite well with the data recorded. Again the resulting PCB resonance frequencies are equal up to the third digit with $f_0 = 14.0\,\text{GHz}$. The Quality factors are around $Q = 90 \pm 40$.

For both cases, no-cut and the cut PCB, the accordance of the resonance frequency f_0 and the Quality factor Q both support the assumption that the examined resonance is indeed a PCB resonance.

3   Simulation

One of the main goals of this thesis was to do a finite element simulation of the device glued on the PCB and mounted inside the sample holder (see Fig. 1 and section 2.1). In a first step we wanted to reproduce the PCB resonance in the simulation for the setting used in the no-cut PCB measurements. Then in a second step we could modify parts of the sample holder or the PCB and analyse the influence on the PCB resonance. This would lead to an understanding of the engineering to control the properties of the PCB resonance and future devices could be designed such that the PCB resonance only minimally disturbs the experiment.

To implement the simulation we used $COMSOL$[1] which is a commercial software solution. Unfortunately it was not possible to realize a working simulation for the device including the sample holder and the PCB. In the following the main problems and limitations encountered are described. For a more detailed account of the simulation procedure see appendix A.

Trace	f_0 [GHz]	Q
No-cut PCB		
S_{12}	9.857	200
S_{34}	9.857	220
S_{23}	9.860	250
S_{14}	9.859	190
Cut PCB		
S_{12}	14.026	130
S_{34}	14.032	54
S_{23}	14.069	78
S_{14}	14.037	94

Tab. 1: PCB resonance frequency f_0 and Quality factor Q obtained form the Lorentzian fitting of the different traces of the PCB resonance for both, the no-cut and cut PCB. The fits are shown in Fig. 6 and Fig. 7.

There are big differences in the length scales of the different structures in the geometry we wanted to simulate. This ranges from the 150 nm thick niobium layer which is used for the fabrication of the CPW resonators with lateral dimensions of the order of $10\,\mu$m, to the length scale of the order of cm for the sample holder, i.e. six orders of magnitude. This provides a great challenge for the meshing process defining the finite volume elements on which the simulation is to run. To get valid results all structures have to be resolved by the mesh. This means that there are also great differences in the sizes of the mesh elements which makes free tetrahedral meshing for the whole geometry at once impossible respectively would lead to a meshing with mesh element size of the smallest structure on the whole geometry and therefore to many elements to solve. The meshing was therefore done separately for different domains and a layered approach was used, where the mesh was first generated on a boundary and then extended to

---

[1]www.comsol.com

the bulk. There were some problems when joining the domains with different mesh element length but this method eventually led to a mesh of the whole geometry.

Simulations run on this mesh, with around $300'000$ elements, would run out of memory when trying to solve with a linear solver the approximately $4'000'000$ coupled linear equations. It was then tried to reduce the meshing points by simplifying the geometry. Also it was tried to use a symmetry plane, even though some structures of the sample holder do not obey it. In total number of mesh elements could not be reduced below $98'000$. This was still not enough to run an eigenvalue solver or a frequency solver giving the whole transmission spectrum.

4   Conclusion

During transmission measurements, unwanted spurious modes were observed which are supported by the printed circuit board (PCB) used for holding circuit QED chips and the superconducting ground plane of the cQED chip. This PCB resonance leads to an unwanted decay channel of the qubit reducing the coherence time of the qubit system. Additionally this decay channel interferes with the coupling of the qubits to the CPW resonator modes used for the readout of the qubits. It was shown that by cutting a hole in the PCB right below the chip this resonance could be shifted to higher frequency. This can be qualitatively explained by a simple capacitance model. The capacitance between the copper plane of the PCB and the niobium ground plane is reduced by cutting a hole in the PCB resulting in an increased resonance frequency assuming it is inversely proportional to the capacitance.

Furthermore it was tried to do a finite element simulation of the chip on the PCB including the sample holder. This simulation could not be realized within this thesis. The main problems encountered were the large difference in structure sizes spanning six orders of magnitude which made meshing of the geometry difficult and led to a high number of mesh elements even after simplifications of the geometry. Due to this the solver would run out of memory during the computation.

For the future it would be interesting to have a working simulation which includes the sample holder. Even a simplified geometry could lead to a better understanding of the PCB resonance which would help designing better devices. But for now we found at least a simple way to push the PCB resonance out of the interesting region.

Acknowledgements

I would like to thank Prof. Dr. A. Wallraff for giving me the possibility to do this semester thesis in his group. My gratitude goes to Dr. M. Mondal who supervised this thesis. He was always open for my questions and introduced me to the lab and the instruments. Further thanks go to P. Kurpiers for answering my questions regarding *COMSOL* and introducing me to the network analyser as well as to the whole QUDEV group. Thanks a lot!

Appendices

A   Simulation Procedure

In this section it is described how the finite element simulation was implemented in *COMSOL* version 4.4 which is a commercial software environment offered by COMSOL Inc.[2] Especially the RF-module was used. For some documentation on *COMSOL* see [12][13]. Fig. 8 shows a screen shot of *COMSOL*. On the left side, in the panel *ModelBuilder*, the different parts of the model are listed and on the right side the geometry is depicted. In the following all steps of the simulation are explained.

The *COMSOL* files of the simulation can be found on the shared (Q:) QUDEV drive under Q:\USERS\Marc\COMSOL\COMSOL sim.
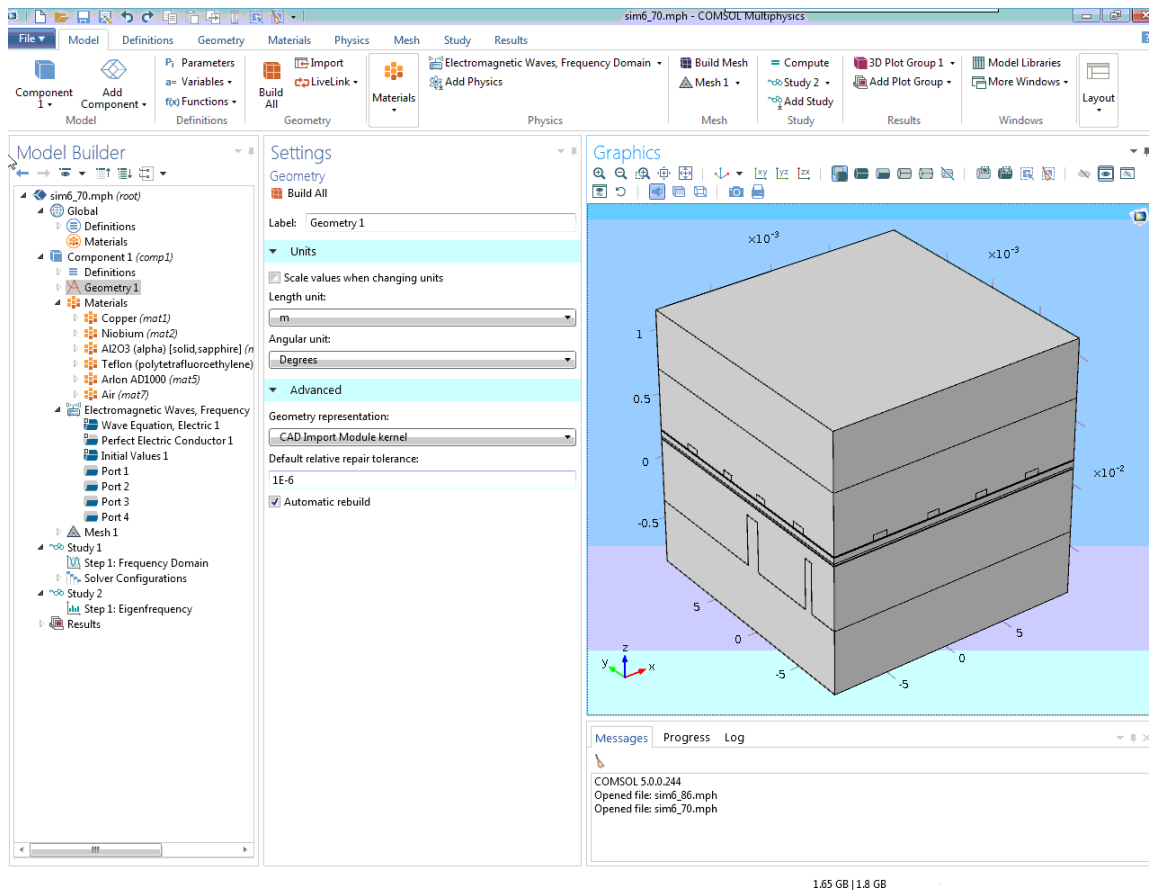

Fig. 8: Illustrative screen shot of *COMSOL*. The panel *ModelBuilder* on the left side lists the different parts of the model. The *Graphics* panel on the right shows the geometry. The *Settings* panel in the middle shows the options for the selected part of the model in the *ModelBuilder* panel.

---

[2]www.comsol.com

A.1   Geometry

The geometry of the sample holder and the cover were both imported from their respective CAD file used for the production of the devices. The PCB was constructed from simple structures in *COMSOL*.

The patterned niobium layer of the chip was at first imported in 2D from the mask used to fabricated the chips, extruded to 3D and put on a block, directly generated in *COMSOL*, representing the sapphire. This import generated lots of unnecessary points along the curves. This could not be repaired with the tools of *COMSOL*. Later when the geometry was simplified in order to reduce the mesh, all structures except the resonators were removed before importing. Even later to further simplify the geometry the resonators were substituted by two simple straight line resonators directly constructed in *COMSOL*. This also solved the problem of the additional points.

All parts were then put together. The bonding wires connecting the resonators on the niobium layer with the corresponding leads on the PCB and the ground planes of the niobium layer and the PCB, were simulated by placing rectangular niobium blocks in the appropriate places. Also we connected the different parts of the niobium ground planes with each other by adding blocks reaching across the two resonators. Then a $2\,\mathrm{cm} \times 2\,\mathrm{cm} \times 2\,\mathrm{cm}$ cube of the whole geometry was cut out with the chip in the center. Simulation should only run on this cube.

To generate the mesh using the layered approach, some additional working planes were added. These planes only split the existing domains in a way allowing for meshing on the boundary and then extruding to the domain leaving the physics untouched.

The final geometry as visualized by *COMSOL* can be seen in Fig. 8 on the right side of the screen shot.

A.2   Materials

The material properties of copper and sapphire ($\mathrm{Al_2O_3}$) were taken form the *COMSOL* material database and were attributed to the corresponding domains of the geometry. For the superconducting niobium a new material was defined with electrical conductivity $\sigma = 10^{25}\,\mathrm{S/m}$, relative permeability $\mu = 10^{-25}$ and relative permittivity $\epsilon = 1$. The same was done for the PCB substrate Arlon AD1000 between the two copper layers with electrical conductivity $\sigma = 7.1 \cdot 10^{-14}\,\mathrm{S/m}$, relative permeability $\mu = 1$ and relative permittivity $\epsilon = 10.7$. All other domains were set to air with properties taken from the *COMSOL* material database.

A.3   Physics: boundary conditions for the electromagnetic wave solver

The physics of the problem was defined using the package 'Electromagnetic Waves , Frequency Domain (emw)' from the RF-module. The 3 standard nodes (see Fig. 8) define all
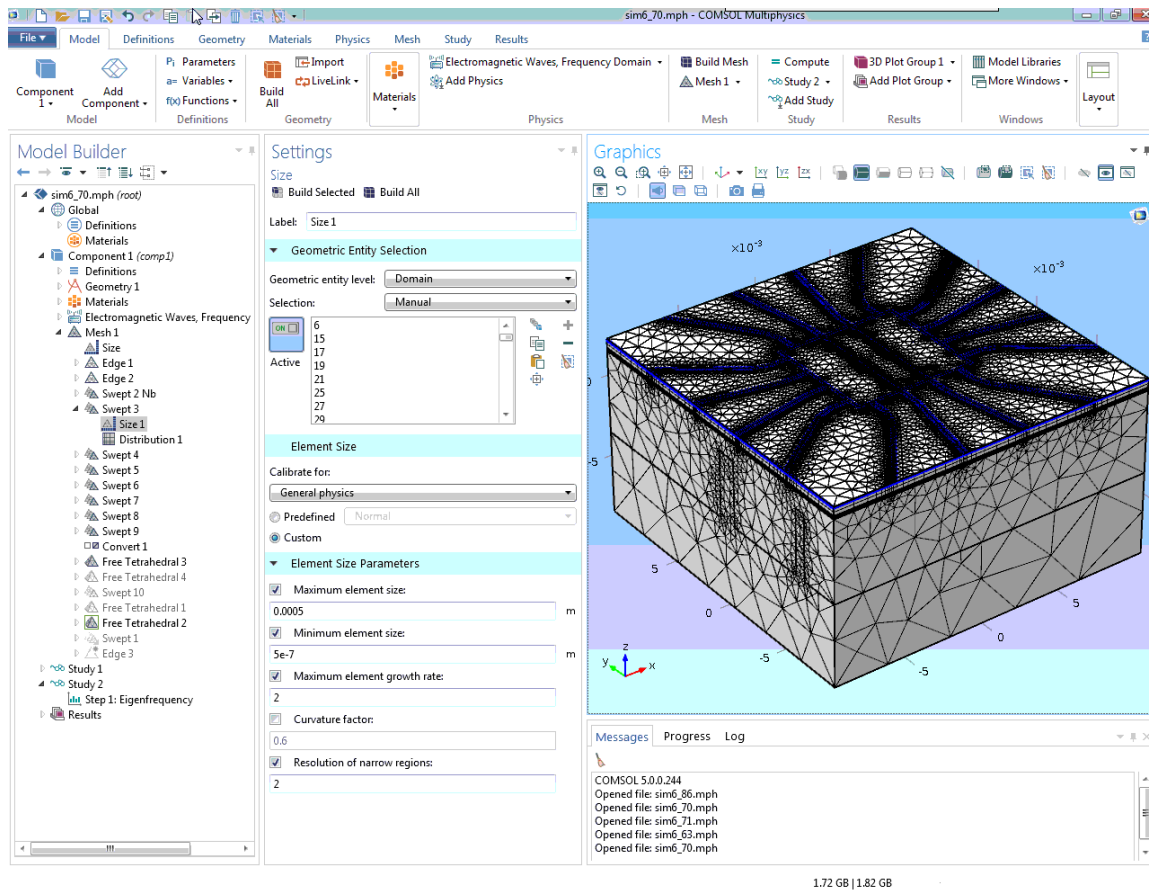
Fig. 9: Screen shot of *COMSOL* illustrating the meshing. The *Graphics* panel on the right shows part of the geometry with applied mesh. The upper part of the geometry has been faded out to allow a view onto the meshing of the inner layers.

exterior boundaries of the geometry to be perfect electric conductors thereby defining them as ground. To allow an excitation of the system four ports were added for the boundaries associated with the PCB lines connected to the resonators. The attributions of the ports override the perfect electric conductor meaning the boundaries of the ports are no longer defined as perfect electric conductors and therefore not grounded. Eventual symmetries can be added here using appropriate boundary conditions.

A.4   Meshing

Fig. 9 shows a screen shot of *COMSOL* illustrating the meshing.

Meshing of the whole geometry in one step by using a free tetrahedral mesh was not possible as described in section 3. Therefore the meshing was done in several steps (see panel *Model Builder* on the right side of screen shot in Fig. 9). First the edges along the resonators were meshed. Subsequently swept meshes – first meshing on the boundary then extruding to the domain – were applied starting form the niobium layer. To do this it was necessary to divide the geometry in layers which was done using work planes as is described

in appendix A.1. This had the disadvantage that the later added swept meshes had to inherit the boundary layers of the already existing meshes which potentially led at some locations to finer respectively coarser meshing than necessary. Therefore it was preferred to use tetrahedral meshing wherever possible. To change at some point to meshing the remaining domains with free tetrahedrals, rectangular mesh faces on the boundaries had to be converted by inserting diagonals.

The software allows you to control individually for each mesh maximum and minimum element size, maximum element growth rate, curvature factor and resolution of narrow regions(see panel *Settings* for the option *Size 1* of the mesh *Swept 3* in the middle of screen shot in Fig. 9).

Meshing was generally very difficult as for the reasons discussed in section 3. There were frequently problems with inverted elements and points which could no be inserted. Especially the joining of the swept to the tetrahedral meshes proved difficult. Also at times the same settings would sometimes fail to generate a mesh and sometimes succeed.

A.5   Study

Two types of studies were tried. Firstly a frequency domain study giving the electric field distribution for a given frequency as well as transmission parameters which is nicely described in ref. [13]. A frequency sweep, i.e. solving the problem for several frequencies, would lead to the desired transmission spectrum. Secondly an eigenfrequency study which returns solely the resonance frequencies and their quality factors Q.

References

[1] C. H. Bennett and G. Brassard, in *Proceedings of IEEE International Conference on Computers, Systems and Signal Processing, Bangalore, India, 1984*, Vol. 1, page 175

[2] M. A. Nielsen and I. L. Chuang, *Quantum Computation and Quantum Information* (Cambridge University Press, 2000)

[3] S. M. Barnett, *Quantum Information* (Oxford University Press, 2009)

[4] Y. Makhlin, G. Schön, and A. Shnirman, Rev. Mod. Phys. **73**, 357 (2001)

[5] J. Koch, T. M. Yu, J. Gambetta, A. A. Houck, D. I. Schuster, J. Majer, A. Blais, M. H. Devoret, S. M. Girvin, and R. J. Schoelkopf, Phys. Rev. A **76**, 042319 (2007)

[6] M. Ansmann, H. Wang, R. C. Bialczak, M. Hofheinz, E. Lucero, M. Neeley, A. D. O'Connell, D. Sank, M. Weides, J. Wenner, A. N. Cleland and J. M. Martinis, Nature(London) **461**, 504 (2009)

[7] J. M. Gambetta and C. T. Rigetti, International Business Machines Corporation, US Patent App. 13/969,780, registered: 19. Aug. 2013, Google Patents US20140167836 A1, [Online] 06.04.2015, `http://www.google.com/patents/US20140167836`

[8] A. Wallraff, D. I. Schuster, A. Blais, L. Frunzio, R. - S. Huang, J. Majer, S. Kumar, S. M. Girvin and R. J. Schoelkopf, Nature(London) **431**, 162 (2004)

[9] A. Wallraff, D. I. Schuster, A. Blais, L. Frunzio, J. Majer, M. H. Devoret, S. M. Girvin, and R. J. Schoelkopf, Phys. Rev. Lett. **95**, 060501 (2005)

[10] M. Sandberg, M. R. Vissers, T. A. Ohki, J. Gao, J. Aumentado, M. Weides and D. P. Pappas, Appl. Phys. Lett. **102**, 072601 (2013)

[11] M. Göppl, A. Fragner, M. Baur, R. Bianchetti, S. Filipp, J. M. Fink, P. J. Leek, G. Puebla, L. Steffen, and A. Wallraff, Journal of Applied Physics **104**, 113904 (2008)

[12] COMSOL Inc., *Intorduction to COMSOL Multiphysics*, [Online] 28.02.2015, `http://www.comsol.com/shared/downloads/IntroductionToCOMSOLMultiphysics.pdf`

[13] COMSOL Inc., *Impedance Matching of a Lossy Ferrite 3-port Circulator*, [Online] 28.02.2015, `http://www.comsol.com/shared/downloads/IntroductionToCOMSOLMultiphysics.pdf`

ETH

Eidgenössische Technische Hochschule Zürich
Swiss Federal Institute of Technology Zurich

Declaration of Originality

This sheet must be signed and enclosed with every piece of written work submitted at ETH.

I hereby declare that the written work I have submitted entitled

Spurious microwave resonance modes of superconducting device

is original work which I alone have authored and which is written in my own words.*

Author(s)

Last name
Röösli

First name
Marc-Philippe

Supervising lecturer

Last name
Wallraff

First name
Andreas

With the signature I declare that I have been informed regarding normal academic citation rules and that I have read and understood the information on 'Citation etiquette' (http://www.ethz.ch/students/exams/plagiarism_s_en.pdf). The citation conventions usual to the discipline in question here have been respected.

The above written work may be tested electronically for plagiarism.

Zürich, 26.05.2015

Place and date

Signature

Print form